AIST Transactions
Vol. 7, No. 3

Strategies for Third-Generation Advanced High-Strength Steel Development

Emmanuel De Moor, Paul J. Gibbs, John G. Speer and **David K. Matlock,** Advanced Steel Processing and Products Research Center, Colorado School of Mines, Golden, Colo. (edemoor@mines.edu, pgibbs@mines.edu, jspeer@mines.edu, dmatlock@mines.edu); and **James G. Schroth,** Research and Development Center, General Motors Corp., Warren, Mich. (james.g.schroth@gm.com)

INTRODUCTION

Over the last several decades, a significant research effort has been directed toward the development of advanced high-strength steel (AHSS) grades. This research was driven mainly by the automotive industry's needs for vehicle weight reduction to improve fuel economy, and increased passenger safety of vehicles. Increased regulatory pressure and consumer expectations regarding crashworthiness[1–2] and fuel economy[3–4] have resulted in extensive usage of AHSS grades in autobody structures. Projections are that the weight percentage of AHSS steel will increase to 35% by 2015, whereas mild steel will decrease from 55% (in 2007) to 29% in bodies and closures of light vehicles.[5] The majority of international and domestic car makers are opting for increased usage of AHSS as part of their vehicle development strategies.[6]

CURRENT AHSS GRADES

The AHSS grades that are currently being applied or are under increased investigation by steel appliers, include dual-phase (DP), complex phase (CP) and transformation induced plasticity (TRIP) steels — referred to as "first generation" AHSS — and the austenitic twinning induced plasticity (TWIP) steels, lightweight steels with induced plasticity (L-IP) and shear band strengthened steels (SIP) of the so-called second generation. (Press-hardenable steels are not considered here.) An overview of representative properties, compared to those exhibited by conventional steel grades, is shown in Figure 1.[7–8] The first-generation AHSS concepts were developed in fairly lean compositions and are primarily ferritic-based multi-phase microstructures. Dual-phase steels are currently the most applied AHSS, which may result, apart from improved strength and formability, from their good weldability and relative ease of processing.[6] Enhanced strength/elongation combinations are clearly obtained for TRIP steel grades, where strain-induced transformation of retained austenite into martensite results in increased strain hardening. The second-generation AHSS steels clearly exhibit superior mechanical properties, but these austenitic grades are highly alloyed, resulting in a significant cost increase. In addition, industrial processing of these alloys, specifically the TWIP steels with high manganese contents, has been shown to be extremely challenging, and the TWIP grades have also been shown to be prone to delayed cracking.[9] Recent research indicates that the embrittlement susceptibility can be reduced by aluminum alloying, although the exact mechanism involved is still under investigation.[9]

From Figure 1, it is clear that a property gap exists between the currently available AHSS grades of the first and second generations. Current research is hence focused on filling this property window using modified or novel processing routes, where special attention should naturally also be given to industrial feasibility and cost-effectiveness.[10–11] An overview of some of the strategies being pursued is presented here. These strategies include:

- Processing to enhance properties of DP steels.
- Modifications to traditional TRIP steel processing.
- Development of high-strength steels with ultrafine bainitic microstructures.
- Implementation of new processing routes, including quenching and partitioning (Q&P) and ultra-rapid heating and cooling.
- Development of high-Mn-content TRIP steels.

DESIGN CONSIDERATIONS FOR THIRD-GENERATION AHSS

Design considerations for third-generation AHSS have been discussed recently using a simplified composite model.[7,12–13] Martensite/ferrite and martensite/austenite microstructures were considered. The results of the calculations obtained by varying the relative phase fractions in hypothetical microstructures are shown in Figure 2, with the individual data points corresponding to fixed relative phase fractions superimposed on the property combinations shown in Figure 1. It

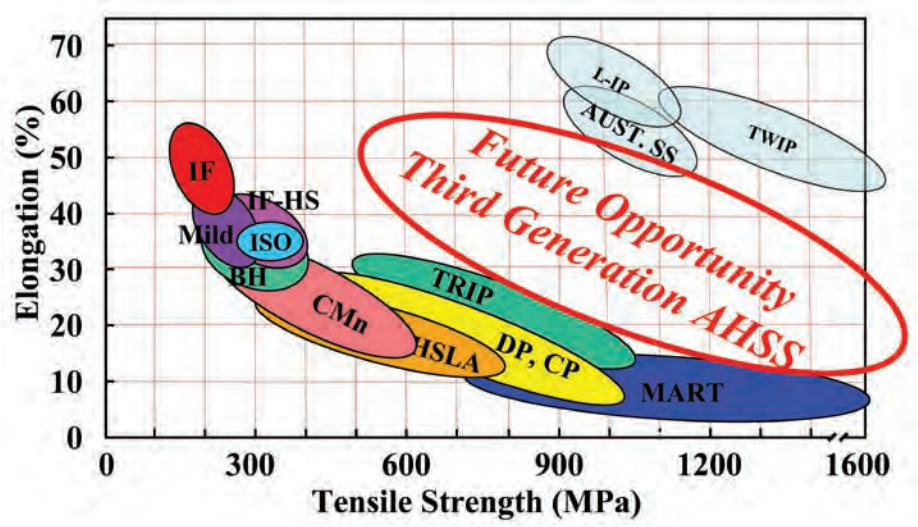

Figure 1
Overview of tensile strength and total elongation combinations for various classes of conventional and advanced high-strength sheet steel (AHSS) grades.[7–8]

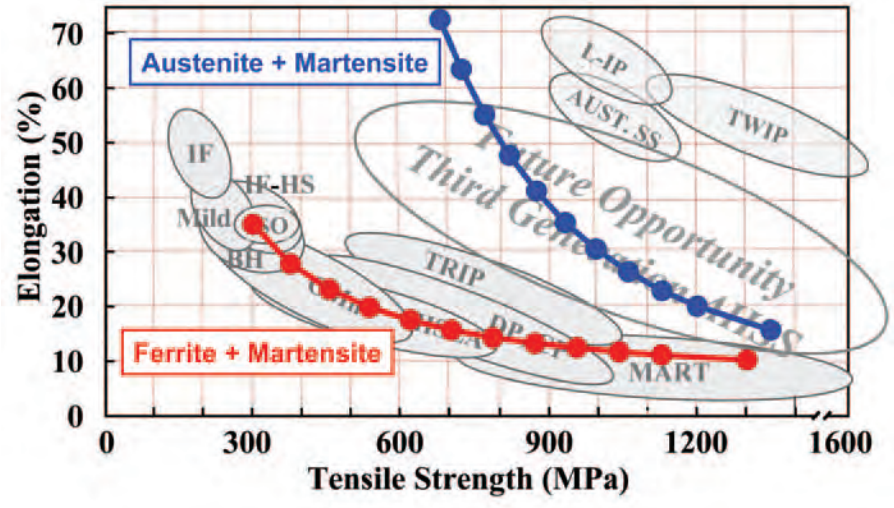

Figure 2
Superposition of the predicted strength/ductility combinations of hypothetical ferrite/martensite and austenite/martensite mixtures.[7,12]

should be noted that the ductility values obtained from the model are uniform elongations. The input parameters to the model are given in Table 1.[14–16] Fully stable austenite was assumed in the results shown in Figure 2, i.e., absence of transformation of the austenite during straining. It is clear that the predicted tensile properties for the hypothetical ferrite/martensite microstructures overlap with the properties exhibited by the first-generation AHSS. The property band corresponding to the austenite/martensite mixtures is situated between the bands of the first- and second-generation AHSS, i.e., within the desired "third generation" regime.

In a second step of the modeling effort, transformation of metastable austenite with strain was included.[12] Four hypothetical austenite stability conditions were considered, as illustrated in Figure 3a. The resulting strength/elongation combination predictions are given in Figure 3b, where the different austenite stability conditions are indicated by letters A through D and the individual data points on each curve correspond to different initial austenite contents (assumed to range from 0 to 85%), with the remainder of the microstructure being ferritic with the properties shown in Table 1. Austenite stability clearly has a pronounced effect on the predicted properties. The lowest stability (condition D) leads to martensite formation at low strains and properties which overlap with the first-generation AHSS band, indicating that the austenite does not significantly contribute to improved properties. The best combinations of strength and ductility are predicted for high volume fractions of relatively stable austenite (curve B in Figure 3b). Simplified assumptions were made in this model, and additional work is ongoing to develop more refined models.[17] However, this fairly straightforward approach provides an understanding of the contribution of the individual constituents and suggests

Table 1
Assumed Tensile Properties for the Constituents Used as Input Parameters for the Model[7]

Constituent	UTS (MPa)	Uniform true strain
Ferrite	300	0.3
Austenite	640	0.6
Martensite	2000	0.08

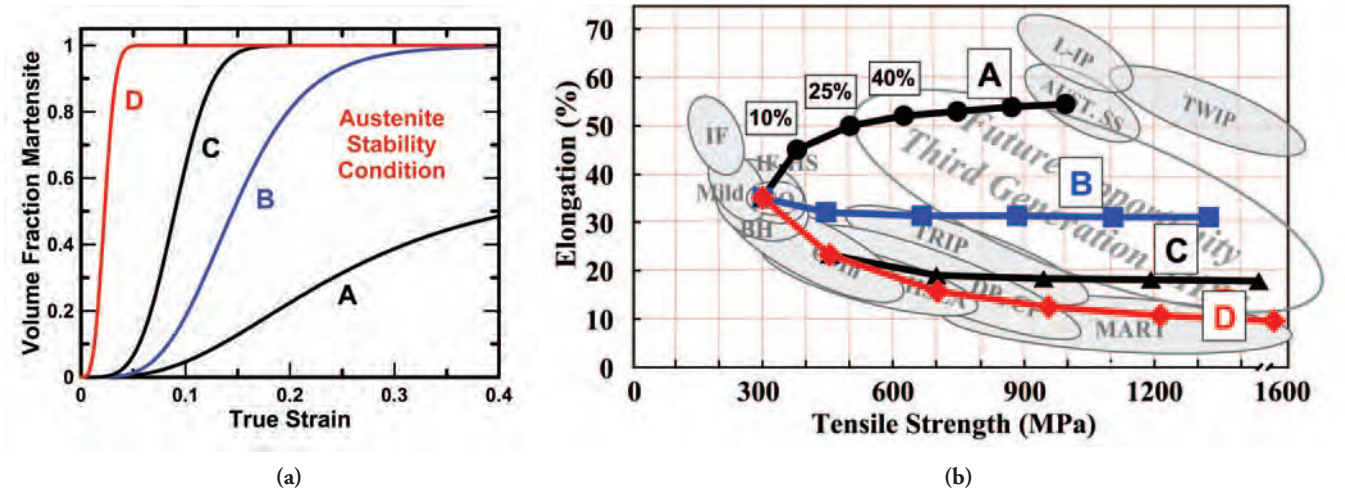

(a) (b)

Figure 3
Effect of austenite stability on predicted mechanical property combinations: (a) four different austenite stabilities were considered, labeled A through D; (b) predicted mechanical property combinations corresponding to the different austenite stabilities. Each data point on a curve corresponds to an initial austenite fraction, considered ranging from 0 to 85%, with the remainder of the initial microstructure being ferrite.[12]

that, in order to obtain the next generation of AHSS steels, complex microstructures are needed consisting of significant fractions of high-strength phases, which may be martensite, bainite or ultrafine-grained ferrite, in combination with highly ductile austenite with controlled stability against transformation of austenite to martensite with strain.

NEXT-GENERATION AHSS DEVELOPMENT APPROACHES

Ongoing AHSS research is focused on increasing strength and/or ductility to higher levels than exhibited by the first-generation AHSS without significantly enriching the alloy compositions, or is aimed at reducing the alloying levels in third-generation AHSS grades. An overview of some of these approaches is discussed here. The proposed compositions used in the different processing paths compiled from literature are summarized in Table 2, and the resulting tensile properties are plotted on a total elongation versus tensile strength diagram in Figure 4a. The solid and dashed lines in the figure are the ferrite-martensite and austenite-martensite property predictions from Figure 2, respectively, shown for reference. It should be recognized that different sample geometries were used in the various studies, and thus some care is needed when comparing mechanical properties. The various sample geometries used are also given in Table 2.

In an effort to enable better comparison of the data generated from the disparate sample geometries represented within prior investigations, the tensile ductilities reported in the literature were adjusted according to ISO 2566/1-1984(E)[18] so that the normalized properties correspond to a single specimen geometry. The values were converted to correspond to those of the standard ASTM E8 geometry with a 50.8-mm (2-inch) gauge length, 12.7-mm (0.5-inch) width and 1-mm thickness, and the results are shown in Figure 4b. The ISO 2566 standard is based on the Oliver formula:[19]

$$A_r = 2A\left(\frac{\sqrt{S_O}}{L_O}\right)^{0.4} \quad \text{(Eq. 1)}$$

with L_O and S_O the original gauge length and cross-sectional area of the specimen, respectively; A_r the elongation on gauge length L_O; and A the elongation on a proportional gauge length of $5.65\sqrt{S_o}$. Conversion of the literature data was done in two steps, with an initial conversion to a proportional gauge length of $5.65\sqrt{S_o}$, followed by conversion to ASTM E8. Adjustment of elongations to a single consistent gauge length resulted in a strength-ductility map significantly different from the one shown in Figure 4a. Many of the samples that displayed high strength/ductility combinations had short and/or circular gauge lengths. After adjusting to predict properties characteristic of a standard sample geometry, many of the results fell into the range exhibited by other materials. However, after the data was replotted, selected studies clearly show properties at the upper boundary of the property band. The different alloying and heat treating approaches associated with Figure 4 are discussed in the following paragraphs.

Enhanced DP Steels

An increase in strength of dual-phase steels can readily be obtained by increasing the martensite volume fraction by altering carbon content and/or intercritical annealing temperature.[12] In this way, DP780 and DP980 have been developed and are currently available commercially. A strength increase has also been obtained by microstructural refinement resulting from special hot deformation practices.[21–29] One such approach, employing deformation induced ferrite transformation (DIFT), is schematically shown in Figure 5. The DIFT methodology involves strain-induced phase transformation from austenite to ferrite by rolling the material approximately 25–50°C above the A_{r3} temperature but below the A_{e3} temperature. This approach has been found successful to produce ultrafine ferrite with a grain size

Table 2
Processing Routes and Chemical Compositions Employed in Different Studies

Process	Composition	Sample Geometry
Enhanced DP	0.17C-1.63Mn-0.28Si[30]	3.5 × 5 mm, GL: 10 mm
Modified TRIP	0.39C-1.16Si-1.20Mn[32]	JIS-5 25 mm wide, GL: 50 mm
	0.38C-1.46Si-1.20Mn[33]	JIS-5 25 mm wide, GL: 50 mm
	0.39C-1.99Si-1.20Mn[33]	JIS-5 25 mm wide, GL: 50 mm
	0.23C-1.65Mn-0.45Si-1.14Al-0.076P-0.085Ti[34]	A80: 20 × 1 mm, GL: 80 mm
	0.24C-1.67Mn-0.45Si-1.38Al-0.080P-0.081Nb[34]	A80: 20 × 1 mm, GL: 80 mm
	0.22C-1.55Mn-1.55Si-0.035Nb[35]	Small specimen test technique based on punching a 3 mm disk out of a 300–350 μm thick specimen[20]
	0.186C-1.53Mn-1.48Si-24ppmTi-1081ppmV-81ppmN[36]	no properties reported
	0.225C-1.58Mn-1.60Si-25ppmTi-1550ppmV-90ppmN[36]	no properties reported
	0.20C-1.51Mn-1.51Si[37]	JIS-13B specimens: 12.5 × 1.2 mm, GL: 50 mm
	0.20C-1.71Mn-1.48Si-0.02Nb[38]	JIS-5 specimens, 25 × 1.2 mm, GL: 50 mm
	0.185C-2.3Mn-1.5Si-0.25Mo[39]	2.5 × 6.25 mm, GL: 150 mm
	0.285C-2.3Mn-1.5Si-0.25Mo[39]	2.5 × 6.25 mm, GL: 150 mm
Bainite	0.79C-1.94Mn-1.59Si-1.33Cr-0.30Mo-0.11V[42]	no properties reported
	0.98C-1.89Mn-1.46Si-1.26Cr-0.26Mo-0.09V[42,44,45]	no properties reported
	0.83C-1.98Mn-1.57Si-1.02Cr-0.24Mo-1.54Co[42,45]	no properties reported
	0.78C-1.95Mn-1.49Si-0.97Cr-0.24Mo-1.60Co-0.99Al[42,45]	no properties reported
	0.80C-2.01Mn-1.59Si-1Cr-0.24Mo-1.51Co[46,49]	5 mm diameter, GL: 25 mm
	0.79C-1.98Mn-1.56Si-1.01Cr-0.24Mo-1.51Co-1.01Al[46,49]	5 mm diameter, GL: 25 mm
	0.43C-3.00Mn-2.02Si[50,51]	Hounsfield no. 11: 3 mm diameter, GL: 50 mm
	0.19C-2.90Mn-2.13Si[50]	Hounsfield no. 11: 3 mm diameter, GL: 50 mm
	1.1C-3.00Mn-2.02Si[50]	Hounsfield no. 11: 3 mm diameter, GL: 50 mm
	0.22C-3.00Mn-2.03Si[51]	Hounsfield no. 11: 3 mm diameter, GL: 50 mm
	0.39C-2.05Si-4.08Ni[51]	Hounsfield no. 11: 3 mm diameter, GL: 50 mm
	0.39C-2.05Si-4.09Ni[52,53]	Hounsfield: 3.5 mm diameter, GL: 20 mm
	0.40C-2.01Si-4.15Ni[52,53]	Hounsfield: 3.5 mm diameter, GL: 20 mm
	0.22C-3.00Mn-2.03Si[52,53]	Hounsfield: 3.5 mm diameter, GL: 20 mm
	0.22C-3.00Mn-1.99Si[52,53]	Hounsfield: 3.5 mm diameter, GL: 20 mm
	0.32C-1.97Mn-1.45Si-1.26Cr-0.26Mo-0.10V[41]	BS EN 10 002-1:1990
	0.31C-1.51Si-1.44Cr-0.25Mo-3.52Ni-0.10V[41]	BS EN 10 002-1:1990
	0.30C-1.51Si-1.42Cr-0.25Mo-3.53Ni[41]	BS EN 10 002-1:1990
	0.31C-1.51Si-1.44Cr-3.52Ni-0.25Mo-0.10V[47]	3 mm diameter, GL: 19 mm
	0.30C-1.51Si-1.42Cr-3.53Ni-0.25Mo[47]	3 mm diameter, GL: 19 mm
	0.29C-2.25Mn-1.50Si-0.26Mo[47]	3 mm diameter, GL: 19 mm
	0.29C-1.97Mn-1.46Si-0.46Cr-0.25Mo[47]	3 mm diameter, GL: 19 mm
	0.29C-1.56Mn-1.49Si-1.47Cr-0.25Mo[47]	3 mm diameter, GL: 19 mm
	0.27C-1.53Mn-1.71Si-1.47Ni-0.17Cr-0.24Mo[47]	3 mm diameter, GL: 19 mm
	0.22C-2.23Mn-1.50Si-0.25Mo[47]	3 mm diameter, GL: 19 mm
	0.21C-1.56Mn-1.46Si-1.49Cr-0.24Mo[47]	3 mm diameter, GL: 19 mm
Quenching & Partitioning	0.20C-1.71Mn-1.48Si-0.02Nb[38]	JIS-5 specimens, 25 × 1.2 mm, GL: 50 mm
	0.19C-1.59Mn-1.63Si[55,56]	sub-size ASTM: 6.34 × 1.2 mm, GL: 25.4 mm
	0.20C-1.63Mn-1.63Si[57,58]	A50: 12.5 × 1 mm, GL: 50 mm
	0.24C-1.61Mn-1.45Si-0.30Al[57,58]	A50: 12.5 × 1 mm, GL: 50 mm
	0.25C-1.70Mn-0.55Si-0.69Al[57,58]	A50: 12.5 × 1 mm, GL: 50 mm
	0.24C-1.60Mn-0.12Si-1.41Al-0.17Mo[57,58]	A50: 12.5 × 1 mm, GL: 50 mm
	0.21C-1.96Mn-1.49Si-0.25Mo[57,58]	A50: 12.5 × 1 mm, GL: 50 mm
	0.17C-1.65Mn-0.38Si-1.11Al-0.08P[59]	A50: 12.5 × 1 mm, GL: 50 mm
	0.2C-1.5Si-1.8Mn[62]	A50: 12.5 × 1 mm, GL: 50 mm
	0.2C-1.6Si-3Mn[60]	ASTM E8: 12.7 × 1 mm, GL: 57.15 mm
	0.29C-1.59Si-2.95Mn[60]	ASTM E8: 12.7 × 1 mm, GL: 57.15 mm
	0.28C-1.64Si-4.95Mn [60]	ASTM E8: 12.7 × 1 mm, GL: 57.15 mm
	0.41C-1.27Si-1.30Mn-1.01Ni-0.56Cr[61]	16 × 1 mm, GL: 80 mm
Flash processing	0.16C-0.16 Si-0.79Mn-0.13Cr-0.08Ni-0.13Cu[63]	not reported
	0.15C-0.21 Si-1.46Mn[63]	not reported
	0.04C-0.16Mn-0.02Cr-0.09Ni[63]	not reported
	0.21C-0.22 Si-0.63Mn-0.33Cr-0.01Ni-0.04Cu[64]	12.7 × 3.1 mm, GL: 50 mm
	0.22C-0.26 Si-1.05Mn-0.22Cr[64]	12.7 × 3.1 mm, GL: 50 mm
	0.21C-0.27Si-0.73Mn-0.48Cr-0.48Ni-0.16Mo-0.18Cu[65]	6.3 × 1.6 mm width, GL: 25 mm
Lower Mn TWIP/TRIP	0.02C-15.8Mn-3.0Si-2.9Al[71]	not reported
	0.04C-20.1Mn-2.8Si-2.9Al[71]	not reported
	0.03C-25.6Mn-3.0Si-2.8Al[71]	not reported
	1.13C-11.4Mn-0.2Si-0.17Ni-0. 08Mo[72]	6.25 mm diameter, GL: 25 mm
High Mn TRIP	0.10C-5.2Mn-0.12Si[73-75]	sub-size ASTM: 6.34 × 1.2 mm, GL: 25.4 mm
	0.10C-5.8Mn-0.13Si[73-75]	sub-size ASTM: 6.34 × 1.2 mm, GL: 25.4 mm
	0.10C-7.1Mn-0.13Si[73-75]	sub-size ASTM: 6.34 × 1.2 mm, GL: 25.4 mm

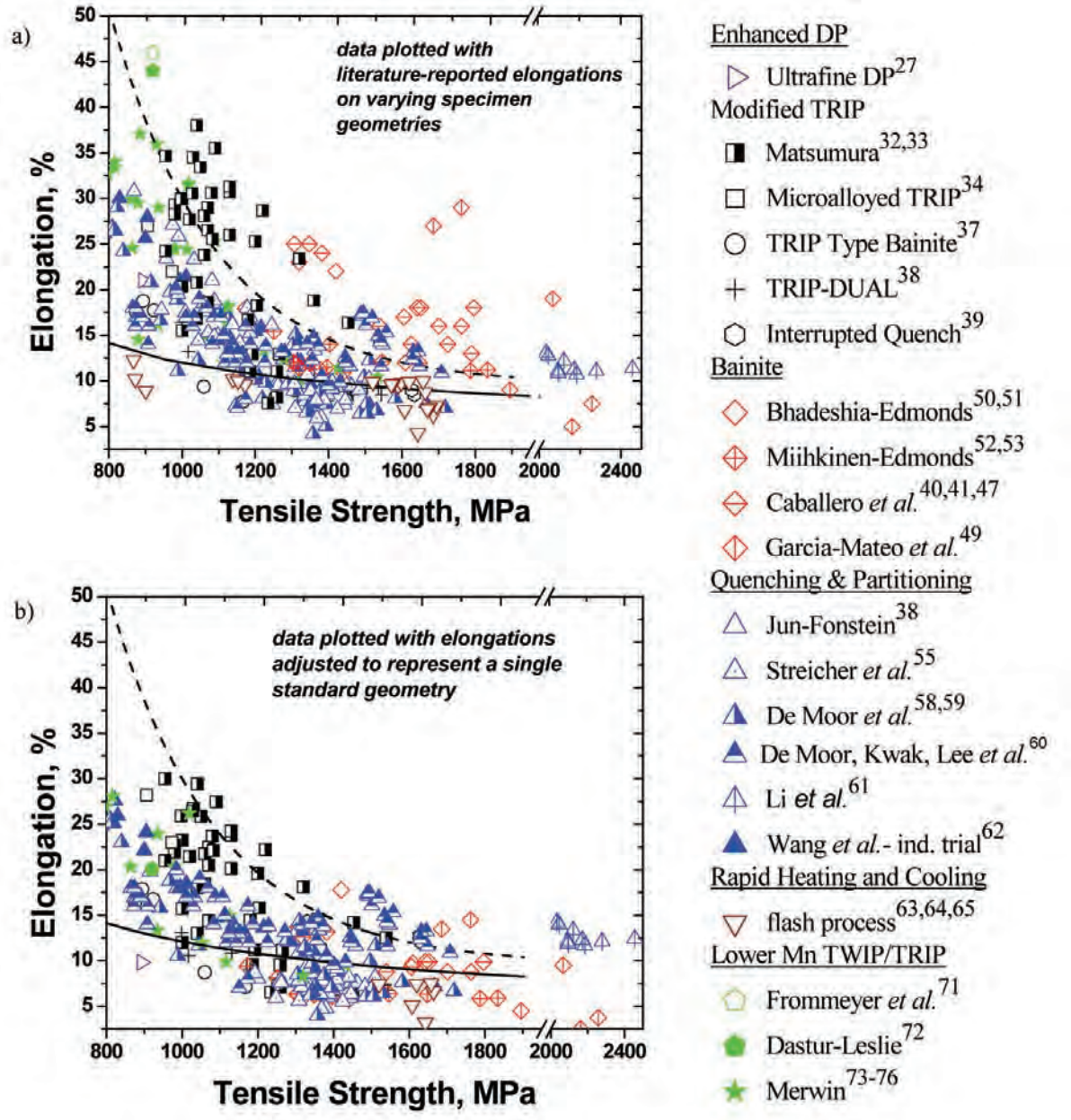

Figure 4
Overview of total elongation and tensile strength combinations obtained by different approaches: (a) data as reported and (b) same data adjusted to ASTM E8 standard specimen geometry. The predicted uniform elongation results for martensite/ferrite (solid line) and martensite/austenite mixtures (dashed line) from Figure 2 are also shown for reference.

on the order of 1 μm. Special cooling practices following deformation have also led to ultrafine DP microstructures in classical DP compositions such as 0.06C-1.9Mn-0.16Mo.[27] (It is interesting to note that an ultrafine DP microstructure was obtained in a leaner composition where the expensive Mo addition was omitted.) Another process consists of a large strain (true strain ~ 1.6) warm deformation below the pearlite finish temperature resulting in an ultrafine-grained ferrite matrix with homogeneously dispersed, spheroidized cementite particles.[30] A grain size of 1–2 μm was obtained which remained essentially stable during subsequent intercritical annealing. A tensile strength level of 893 MPa combined with 21% elongation was reported for ultrafine-grained DP in this way.[30] However, these properties remain within the first generation AHSS band, and thus microstructural refinement in DP steels does not offer an opportunity to produce third-generation AHSS properties. Strength increase has, in some cases, not been the primary focus, and a variety of DP microstructures have been developed, aiming at satisfying specific requirements such as high hole expansion or bendability rather than increasing tensile properties.[31]

Modified TRIP Steels

Early TRIP steel research was performed on grades with higher carbon contents than currently used in commercially available grades. Matsumura et al. investigated 0.4CMnSi grades,[32–33] and it is apparent from Figure 4 that the high

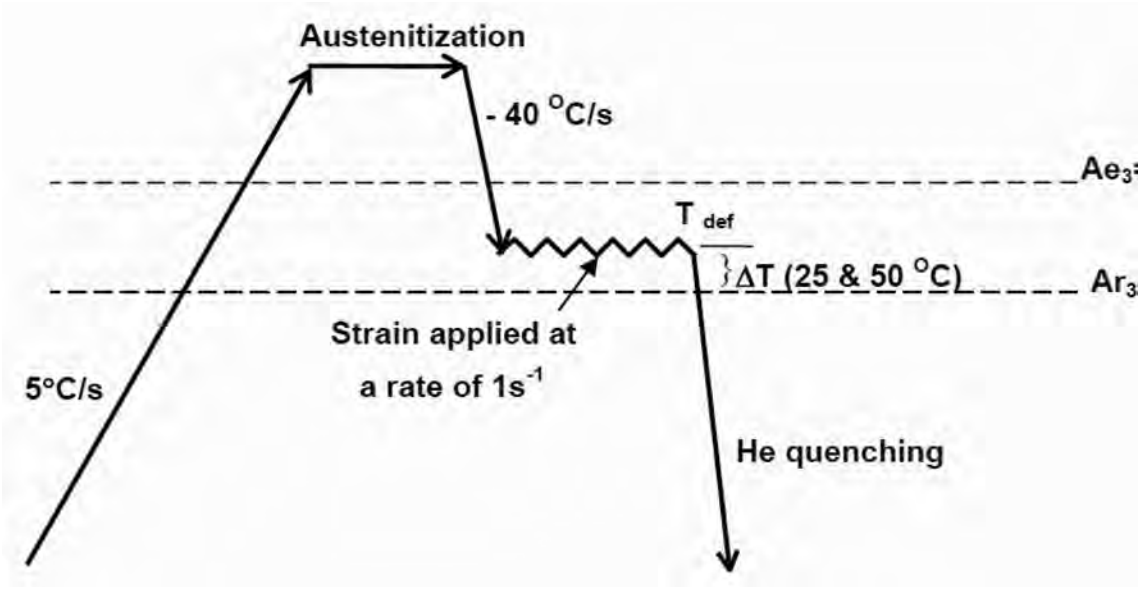

Figure 5
Thermomechanical processing path for deformation-induced ferrite transformation.[29]

carbon level results in properties that merit consideration in the context of third-generation AHSS objectives. Grain refinement of TRIP steels by microalloying has also been investigated.[34–36] Tensile strength levels up to 1 GPa with ductility levels of about 20% total elongation have been obtained, as shown in Figure 4. Other TRIP steel developments involve modified heat treating, where isothermal holding following full austenitization is done at various temperatures (350–475°C), and in some cases below the M_S temperature (calculated to be 417°C).[37] Lowering the holding temperature resulted in increased strength levels and reduced ductility associated with less pronounced strain hardening, as shown in Figures 6a and 6b, respectively. Isothermal holding below the M_S temperature is also applied in the TRIP-dual[38] and interrupted quenching[39] processes, resulting in the properties shown in Figure 4 (where the holding temperature is below M_S, these concepts may incorporate elements of "one-step" Q&P, discussed below). Significant fractions of austenite, assumed to result from a bainite transformation, are retained in these microstructures.

Ultrafine Bainite

Recent work has been conducted to create ultrafine bainitic microstructures.[40–48] Theoretical calculations based on the T'_0 concept have led to a judicious alloying basis, shown in Table 2, to obtain the desired fine-scale microstructure and absence of large blocks of untransformed austenite which may affect toughness adversely. The T_0 curve is the locus of all points where austenite and ferrite of the same chemical composition have the same free energy plotted on a temperature-versus-carbon concentration diagram. The T'_0 curve is similarly defined but takes into account the stored strain energy of the bainitic ferrite. Low transformation temperatures in the range of 125–325°C were employed, leading to microstructures as shown in Figure 7 for a 0.98C-1.89Mn-1.46Si-1.26Cr-0.26Mo-0.09V alloy. The steel shown in Figure 7 exhibited 600 HV hardness and strength in excess of 2.5 GPa. The microstructure was obtained after a 15-day heat treatment, a time which may be too long for industrial purposes, and thus further work has been done on increasing bainite kinetics, reducing heat treatment to hours rather than days by alloying with Al and/or Co.[45,49] The combination of high strength and toughness has made this material a strong candidate for armor applications at a significantly lower cost than maraging steels with similar properties. Tensile strength levels in the 1,700–2,300 MPa range were obtained with pronounced tensile elongation and toughness. Small specimens were used (3 mm ø × 19 mm GL) in these studies, and the elongation conversion

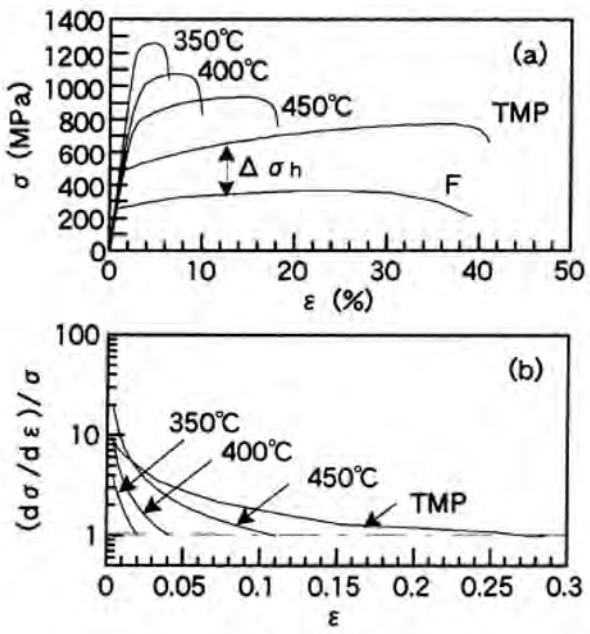

Figure 6
Effect of isothermal holding temperature for a fixed time of 200 seconds following full austenitization of a 0.20C-1.51Mn-1.51Si steel with an estimated M_s temperature of 417°C on (a) the stress-strain curves and (b) strain hardening plots. TMP refers to a TRIP-type multiphase steel austempered at 400°C for 1,000 seconds after an intercritical anneal at 780°C for 1,200 seconds. F represents a 0.006C-1.50Si-1.50Mn ferritic steel.[37]

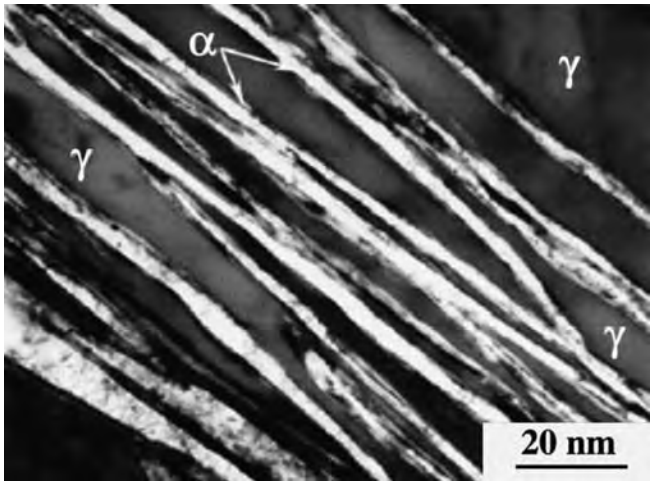

Figure 7
Transmission electron micrograph of a very fine bainitic microstructure developed in a 0.98C-1.89Mn-1.46Si-1.26Cr-0.26Mo-0.09V alloy at a temperature of 200°C for 15 days.[42]

to an ASTM E8 geometry suggests that these materials would exhibit property combinations characteristic of the high-strength first-generation steels shown in Figure 1, albeit at higher strength levels. Given the relatively higher alloy and carbon levels, this approach may be more difficult to implement in high-volume vehicle applications, although bainitic microstructures have also been obtained in leaner alloys.[40–41,47,50–53]

Quenching and Partitioning

Quenching and partitioning (Q&P) has been proposed recently as a new way of producing martensitic steels containing enhanced levels of retained austenite.[54] The process consists of a two-step thermal treatment and is schematically shown in Figure 8a: after soaking, the steel is quenched to a predetermined temperature (quench temperature, QT) in the M_s–M_f range to produce a partially martensitic, partially austenitic microstructure. The second, so-called partitioning step aims at carbon enrichment of the austenite by (partial) carbon depletion of the martensite and carbon transport to the austenite. Thus, carbon-stabilized austenite is retained in the microstructure after final quenching to room temperature. Partitioning can be done at a higher temperature than the QT, via so-called two-step Q&P, or by holding at the quench temperature, called one-step Q&P. The quench temperature can be calculated, which stabilizes the maximum amount of austenite using carbon present in the martensite, as illustrated in Figure 8b. The calculation applies the Koistinen-Marburger relationship to calculate the initial martensite fraction formed by quenching to the QT, and again to calculate the martensite fraction that forms upon final quenching to room temperature following carbon partitioning.[54] Full carbon depletion of the initially formed martensite is assumed in the original model. Retained austenite stabilization is hence believed to result from carbon depletion of martensite, rather than from bainite transformation. Carbide precipitation should be suppressed, and Si-containing TRIP steel–type compositions have shown promise for Q&P processing.[55–56] The addition of molybdenum retards bainite transformation kinetics and has been shown to increase the retained austenite volume fraction, whereas aluminum substitution for silicon has been found to accelerate the bainite reaction, and reduce the retained austenite fractions.[57] High retained austenite fractions are believed to result in improved strength and ductility, as shown in Figure 4.[55,58–61] Mechanical properties reported from a recent industrial trial are also shown in Figure 4.[62]

Rapid Heating and Cooling

A very rapid heating and cooling approach, similar to induction hardening, has been applied to sheet steel.[63–65] Very short heating and cooling times and corresponding very fast heating and cooling rates are used. Microstructural characterization of an AISI 8620 grade processed by this so-called "flash process" revealed a very fine microstructure

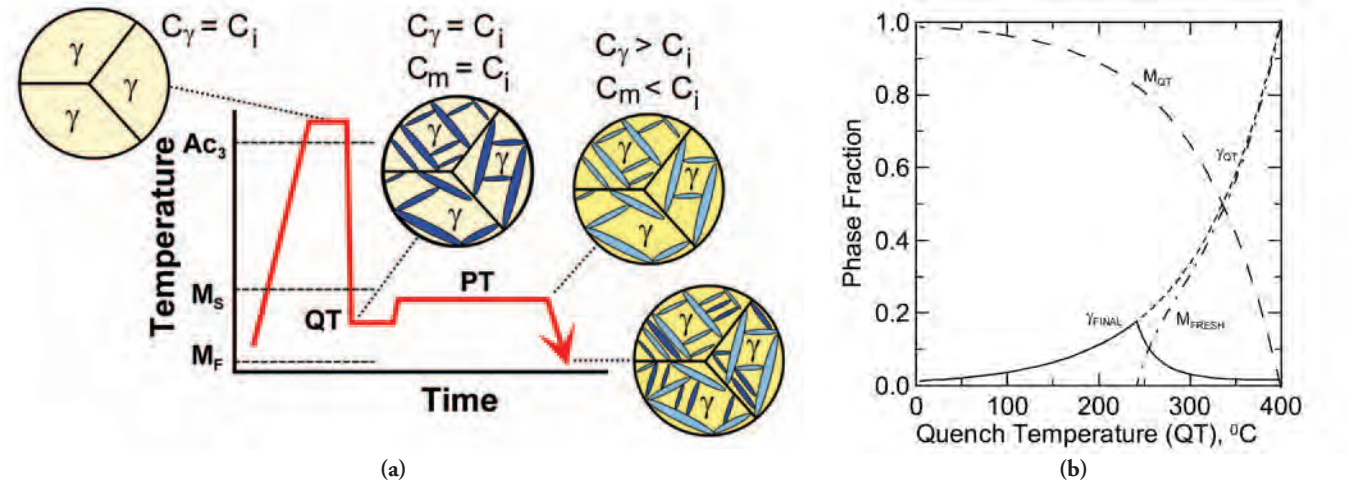

Figure 8
(a) Schematic illustration of the quenching and partitioning process; and (b) calculation of the optimal quench temperature resulting in the greatest austenite fractions by applying the Koistinen-Marburger equation to the initial and final quench assuming full carbon partitioning between the martensite and austenite.[54]

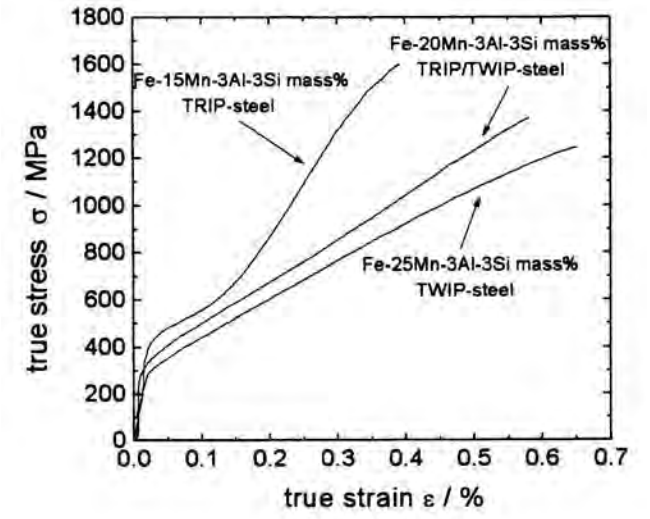

Figure 9
True stress versus true strain curves showing the effect of Mn content on strain hardening.[71]

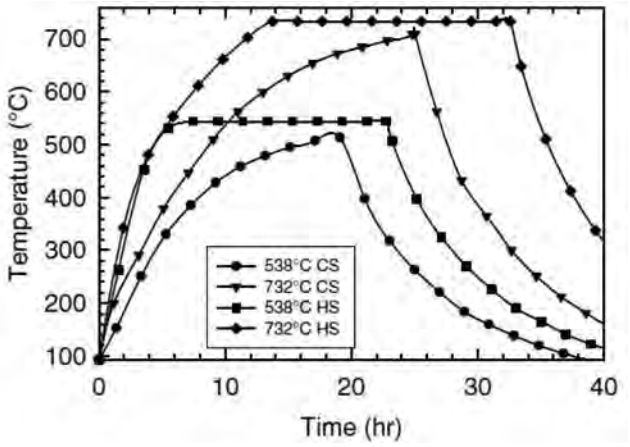

Figure 10
Batch annealing cycles applied by Merwin in 0.1C-5/7Mn steels to obtain Mn enrichment of austenite, thus stabilizing significant austenite fractions at room temperature. The temperature cycles are shown for cold spot (CS) and hot spot (HS).[73]

consisting of bainitic ferrite and martensite with a uniform distribution of large and small carbides believed to be Cr-rich cementite.[65] These carbides have been suggested to be undissolved carbides inherited from the prior microstructure due to the very short austenitizing times. A very fine prior austenite grain size is also observed in the final microstructure. It has been hypothesized that the short dwell times above the A_{c3} temperature may result in incomplete carbon diffusion and redistribution throughout the austenite, which may lead to complex austenite decomposition into different transformation products such as bainite and martensite.[65] High strengths are achievable, although it is not clear from the results in Figure 4 that this approach would offer any unique property advantages.

Lower-Mn TWIP/TRIP

A variety of compositions have been proposed for the second-generation austenitic steel grades, including:

- 15, 20, 25, 30Mn-2, 3, 4Si-2, 3, 4Al-0.01, 0.02, 0.03, 0.04, 0.06C.[66]
- 27Mn-0.02C.[67]
- 30Mn-3Al-3Si.[68]
- 16, 18, 19Mn-6, 7, 8, 10Cr-0.25C-0.080, 0.100, 0.150, 0.200N.[69]

Some of the current research is focusing on reducing the alloying content in these grades.[70] Frommeyer et al. investigated Fe-Mn-3Si-3Al steel grades with lower Mn content (15% Mn), as shown in Table 2.[71] The effect of lowering the Mn content from 25 to 15 wt. % on the stress-strain behavior is shown in Figure 9. A clear effect is observed at true strains exceeding 0.15, where a pronounced increase in strain hardening is observed in the 15Mn steel, which is believed to be associated with α' martensite transformation. No transformation products, α' nor ε martensite, were observed in the 25Mn steel, and the strain hardening resulted predominantly from twin formation. The 20Mn steel exhibited twinning as well as transformation induced strain hardening. It can be noted that the mechanical properties in the 15Mn-3Si-3Al grade are similar to the properties exhibited by a 1.1C-11.4Mn Hadfield steel,[72] also shown in Figure 4.

High-Mn TRIP

An alternative processing concept has been proposed by Merwin,[73–76] based on earlier work by Grange and Miller,[77–78] to produce duplex ferrite-austenite microstructures based on "low" manganese (5–7 wt. %), low-carbon (0.1 wt. %) compositions, as shown in Table 2. These Mn levels are higher than conventional sheet products, but much lower than in TWIP grades. Conventional hot rolling, cold rolling and batch annealing processes were employed. Example annealing cycles are shown in Figure 10. Prolonged holding at the peak annealing temperature results in an intercritical anneal where manganese partitioning occurs. An ultrafine microstructure consisting of ferrite and high-manganese austenite is obtained at room temperature. Austenite fractions up to 17% were measured in the 0.10C-5.2Mn steel, whereas austenite levels up to 28% and 38% were obtained in the 0.10C-5.8Mn and 0.10C-7.1Mn

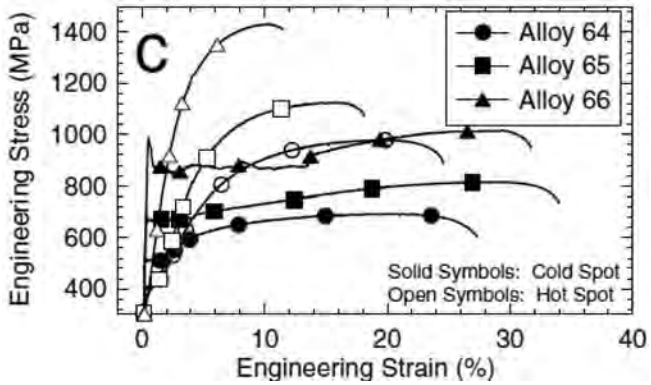

Figure 11
Example engineering stress-strain curves obtained in the 0.10C-5.2Mn (alloy 64), 0.10C-5.8Mn (alloy 65) and 0.10C-7.1Mn (alloy 66) steels after Mn enrichment of the austenite by the batch annealing cycles shown in Figure 10.[73]

grades, respectively. Pronounced strain hardening was obtained, as shown in Figure 11, for selected annealing conditions. Apart from the benefit of reducing alloying relative to TWIP steels, this approach may also show promise for those facilities that do not possess continuous annealing or advanced cooling capabilities.

CONCLUDING PERSPECTIVES

Model predictions provide important guidance in identifying successful approaches for next-generation advanced high-strength steels. It was shown previously that multi-phase microstructures with a high-strength constituent such as martensite, bainite or ultrafine ferrite will be needed, along with a ductile austenite constituent with good work hardening characteristics. A newer model to incorporate the effects of the mechanical stability of the austenite on the strain hardening behavior indicates that new strategies to control the austenite morphology and stability will also be helpful in optimizing the contribution of the austenite to tensile ductility and other formability measures.

A number of metallurgical approaches for advanced high-strength steel development from the recent literature were reviewed here, and these approaches are generally consistent with directions identified by the model results. The reported strategies have employed a variety of means to promote austenite retention and high strength, through alloying and/or processing variations. Strength has been promoted by incorporating low-temperature transformation products, e.g., bainite and martensite, along with new approaches to further refine the microstructure. Austenite content has been promoted via the use of austenite stabilizers, particularly manganese and carbon, along with processing routes to control the scale and morphology of the microstructure, and the composition and stability of the austenite. Some of these product development strategies have been implemented on a limited basis in industry, or are being evaluated through industrial production trials, including applications currently involving hot-stamped components. Comparison of mechanical property results in the available literature points out a broad range of properties across the spectrum of strength/ductility combinations, and highlights the need to consider carefully the specimen geometry when making comparisons of results from different laboratories.

It is clear from this review that several interesting alloy and processing routes exist for potentially producing third-generation AHSS products. However, all will require careful control of alloy additions along with processing times and temperatures, and commercial implementation may require equipment modifications to meet the challenging processing requirements. Some of the development strategies that lead to the most impressive ranges of properties also involve rather elevated levels of carbon and sometimes manganese. Such alloying approaches have typically been avoided in the past for automotive applications due to spot welding considerations, but improved resistance spot welding technology and alternate joining technologies will be introduced to serve as manufacturing enablers if the performance imperative is sufficient. While this review has focused on the broad target of improved strength/ductility combinations, it is likely that other characteristics, such as edge stretching behavior,[79–80] bending and shear fracture,[81–83] delayed cracking,[84–86] etc., will play a greater role in defining optimized materials as matrix strength levels increase further.

ACKNOWLEDGMENTS

The authors gratefully acknowledge the support of the sponsors of the Advanced Steel Processing and Products Research Center, an industry/university cooperative research center at the Colorado School of Mines, and the National Science Foundation through award number CCMI-0729114. Special thanks go to Dave Hanlon, Corus Research, Development and Technology, for helpful discussions.

REFERENCES

1. www.nhtsa.dot.gov.
2. www.euroncap.com.
3. "Setting Emission Performance Standards for New Passenger Cars as Part of the Community's Integrated Approach to Reduce CO_2 Emissions From Light-Duty Vehicles," Regulation (EC) No. 443/2009 of the European Parliament and of the Council, April 23, 2009.
4. "Average Fuel Economy Standards Passenger Cars and Light Trucks Model Year 2011," DOT, NHTSA, Docket No. NHTSA-2009-0062, March 23, 2009.
5. "Progress in Implementation of Advanced High-Strength Steels Into Vehicle Structures," J.R. Fekete, J.N. Hall, D.J. Meuleman and M. Rupp, *Proc. of the Intl. Conf. on New Developments in Advanced High-Strength Sheet Steels*, AIST, June 15–18, 2008, Orlando, Fla., pp. 249–256.
6. L. Brooke and H. Evans, "Lighten Up!" *Automotive Engineering International*, March 2009, pp. 16–22.
7. D.K. Matlock and J.G. Speer, "Design Considerations for the Next Generation of Advanced High-Strength Sheet Steels," *Proc. of the 3rd International Conference on Structural Steels*, ed. by H.C. Lee, the Korean Institute of Metals and Materials, Seoul, Korea, 2006, pp. 774–781.
8. "Advanced High-Strength Steel (AHSS) Application Guidelines," *International Iron and Steel Institute*, Committee on Automotive Applications, www.worldautosteel.org.
9. S-K. Kim, G. Kim and K-G. Chin, "Development of High-Manganese TWIP Steel With 980 MPa Tensile Strength," *Proc. of the Intl. Conf. on New Developments in Advanced High-Strength Sheet Steels*, AIST, June 15–18 2008, Orlando, Fla., pp. 249–256.
10. D.K. Matlock, P.J. Gibbs, J.G. Speer, R.H. Wagoner and J.G. Schroth, "Austenite Preconditioning as an Approach to Enhance Formation of Retained Austenite in Advanced High-Strength Steels," *Proc. NSF CMMI Research and Innovation Conference*, Honolulu, Hawaii, NSF, Washington, D.C., paper for Grant No. 0729114, 8 pages, 2009.
11. D.K. Matlock and J.G. Speer, "Processing Opportunities for New Advanced High-Strength Sheet Steels," *Materials and Manufacturing Processes,* Vol. 25, Issue 1, 2010, pp. 7–13.
12. Ibid., "Third Generation of AHSS: Microstructure Design Concepts," *Microstructure and Texture in Steels and Other Materials*, eds. A. Haldar, S. Suwas and D. Bhattacharjee, Springer, London, 2009, pp. 185–205.

13. S.T. Mileiko, "The Tensile Strength and Ductility of Continuous Fiber Composites," *J. of Materials Science*, Vol. 4, 1969, pp. 974–977.

14. G. Frommeyer, U. Brüx and P. Neumann, "Supra-Ductile and High-Strength Manganese-TRIP/TWIP Steels for High-Energy Absorption Purposes," *ISIJ Intl.*, Vol. 43, No. 3, 2003, pp. 438–446.

15. R.G. Davis, "The Mechanical Properties of Zero-Carbon Ferrite-Plus-Martensite Structures," *Metall. Trans. A*, Vol. 9A, 1978, pp. 451–455.

16. Ibid., "The Deformation Behavior of a Vanadium-Strengthened Dual-Phase Steel," *Metall. Trans. A*, Vol. 9A, 1978, pp. 41–52.

17. H. Nam Han, C.S. Oh, G. Kim and O. Kwon, "Design Method for TRIP-Aided Multiphase Steel Based on a Microstructure-Based Modeling for Transformation-Induced Plasticity and Mechanically Induced Martensitic Transformation," *Mat. Sci. and Eng. A*, Vol. 499, 2009, pp. 462–468.

18. International Organization for Standardization, "Steel — Conversion of Elongation Values — Part 1: Carbon and Low-Alloy Steels," International Standard ISO 2566/1-1984(E), pp. 1–28.

19. D.A. Oliver, *Proceedings of the Institution of Mechanical Engineers*, Vol. 11, 1928, p. 827.

20. G.E. Lucas, "Review of Small Specimen Test Techniques for Irradiation Testing," *Metall. Trans. A*, Vol. 21A, 1990, pp. 1105–1119.

21. R. Song, D. Ponge, D. Raabe, J.G. Speer and D.K. Matlock, "Overview of Processing, Microstructure and Mechanical Properties of Ultrafine-Grained bcc Steels," *Mat. Sci. Eng. A*, Vol. 441, 2006, pp. 1–17.

22. Y. Okitsu, T. Naito, N. Takaki, T. Sugiura and N. Tsuji, "Mechanical Properties and Crashworthiness of Ultrafine-Grained Multi-Phase Steel Sheets for Automotive Body Applications," *Proc. of SAE 2010 World Congress*, SAE Intl., 2010-01-0438, Detroit, Mich.

23. Y. Okitsu, N. Takata and N. Tsuji, "A New Route to Fabricate Ultrafine-Grained Structures in Carbon Steels Without Severe Plastic Deformation," *Scripta Mat.*, in press.

24. Ibid., "Mechanical Properties of Ultrafine-Grained Ferritic Steel Sheets Fabricated by Rolling and Annealing of Duplex Microstructures," *J. Mater. Sci.*, Vol. 43, No. 23–24, 2008, pp. 7391–7396.

25. J.K. Choi, D.H. Seo, J.S. Lee, K.K. Um and W.Y Choo, "Formation of Ultrafine Ferrite by Strain-Induced Dynamic Transformation in Plain Low-Carbon Steel," *ISIJ Intl.*, Vol. 43, No. 5, 2003, pp.746–754.

26. M. Delincé, Y. Bréchet, J.D. Embury, M.G.D. Geers, P.J. Jacques and T. Pardoen, "Structure-Property Optimization of Ultrafine-Grained Dual-Phase Steels Using a Microstructure-Based Strain Hardening Model," *Acta Mat.*, Vol. 55, 2007, pp. 2337–2350.

27. M. Mukherjee, S.S. Harza and M. Militzer, "Grain Refinement in Dual-Phase Steels," *Metall. Trans. A*, Vol. 40A, 2009, pp. 2145–2159.

28. K. Mukherjee, S. Hazra and M. Militzer, "Grain Refinement in Hot Rolled Dual-Phase Steels," *Proc. of SAE 2006 World Congress*, SAE Intl., SP-2035, Detroit, Mich., 2006, pp. 81–86.

29. M. Militzer, S. Sarkar, K. Mukherjee, H. Azizi-Alizamini and W.J. Poole, "Advanced Steels With Complex Ultrafine-Grained Microstructures," *Proc. of New Developments on Metallurgy and Applications of High-Strength Steels*, Buenos Aires, ed. T. Perez, TMS, May 26–28, 2008.

30. M. Calcagnotto, D. Ponge and D. Raabe, "Ultrafine-Grained Ferrite/Martensite Dual-Phase Steel Fabricated by Large Strain Warm Deformation and Subsequent Intercritical Annealing," *ISIJ Intl.*, Vol. 48, 2008, No. 8, pp. 1096–1101.

31. N. Pottore, N. Fonstein, I. Gupta and D. Bhattacharya, "A Family of 980 MPa Tensile Strength Advanced High-Strength Steels With Various Mechanical Property Attributes," *Proc. of the Int. Conf. on Advanced High-Strength Sheet Steels for Automotive Applications*, AIST, June 6–9, 2004, Winter Park, Colo., pp. 119–129.

32. O. Matsumura, Y. Sakuma and H. Takechi, "Enhancement of Elongation by Retained Austenite in Intercritical Annealed 0.4C-1.5Si-0.8Mn Steel," *Trans. ISIJ,* Vol. 27, 1987, pp. 570–579.

33. O. Matsumura, Y. Sakuma, Y. Ishii and J. Zhao, "Effect of Retained Austenite on Formability of High-Strength Sheet Steels," *ISIJ Intl.*, Vol. 32, No. 10, 1992, pp. 1110–1116.

34. D. Krizan, B.C. De Cooman and J. Antonissen, "Retained Austenite Stability in the Cold Rolled CMnAlSiP Micro-Alloyed TRIP Steels," *Proc. of the Int. Conf. on Advanced High-Strength Sheet Steels for Automotive Applications*, AIST, June 6–9, 2004, Winter Park, Colo., pp. 205–216.

35. A. Zarei Hanzaki, P.D. Hodgson and S. Yue, "Hot Deformation Characteristics of Si-Mn TRIP Steels With and Without Nb Microalloy Additions," *ISIJ Intl.*, Vol. 35, No. 3, 1995, pp. 324–331.

36. F. Perrard and C. Scott, "Vanadium Precipitation During Intercritical Annealing in Cold Rolled TRIP Steels," *ISIJ Intl.*, Vol. 47, No. 8, 2007, pp. 1168–1177.

37. K. Sugimoto, T. Iida, J. Sakaguchi and T. Kashima, "Retained Austenite Characteristics and Tensile Properties in a TRIP-Type Bainitic Sheet Steel," *ISIJ Intl.*, Vol. 40, No. 9, 2000, pp. 902–908.

38. H.J. Jun and N. Fonstein, "Microstructure and Tensile Properties of TRIP-Aided CR Sheet Steels: TRIP, Dual and Q&P," *Proc. of the Intl. Conf. on New Developments in Advanced High-Strength Sheet Steels*, AIST, June 15–18, 2008, Orlando, Fla., pp. 155–168.

39. S. Cobo, C. Colin and S. Alain, "Effects of Low-Temperature Heat Treatments on Microstructures and Properties of 0.2–0.3%C Cold Rolled Martensitic Steels," *Proc. of New Developments on Metallurgy and Applications of High-Strength Steels*, Buenos Aires, ed. T. Perez, TMS, May 26–28, 2008.

40. F.G. Caballero, H.K.D.H. Bhadeshia, K.J.A. Mawella, D.G. Jones and P. Brown, "Design of Novel High-Strength Bainitic Steels: Part 1," *Mat. Sci. and Tech.*, May 2001, Vol. 17, pp. 512–516.

41. Ibid., "Design of Novel High-Strength Bainitic Steels: Part 2," *Mat. Sci. and Tech.*, May 2001, Vol. 17, pp. 517–522.

42. F.G. Caballero and H.K.D.H. Bhadeshia, "Very Strong Bainite," *Current Opinion in Solid State and Materials Science*, Vol. 8, 2004, pp. 251–257.

43. C. García-Mateo, F.G. Caballero and H.K.D.H. Bhadeshia, "Low-Temperature Bainite," *J. de Physique IV*, Vol. 112, 2003, pp. 285–288.

44. Ibid., "Development of Hard Bainite," *ISIJ Intl.*, Vol. 43, No. 8, 2003, pp. 1238–1243.

45. Ibid., "Acceleration of Low-Temperature Bainite," *ISIJ Intl.*, Vol. 43, No. 11, 2003, pp. 1821–1825.

46. C. Garcia-Mateo and F.G. Caballero, "The Role of Retained Austenite on Tensile Properties of Steels With Bainitic Microstructures," *Materials Trans.*, Vol. 46, No. 8, 2005, pp. 1839–1846.

47. F.G. Caballero, M.J. Santofimia, C. García-Mateo, J. Chao and C. García de Andrés, "Theoretical Design and Advanced Microstructure in Super High-Strength Steels," *Materials and Design*, Vol. 30, Issue 6, 2009, pp. 2077–2083.

48. F.G. Caballero, J. Chao, J. Cornide, C. García-Mateo, M.J. Santofimia and C. Capdevila, "Toughness Deterioration in Advanced High-Strength Bainitic Steels," *Mat. Sci. and Eng. A*, Vol. 525, Issue 1–2, 2009, pp. 87–95.

49. C. Garcia-Mateo and F.G. Caballero, "Ultrahigh-Strength Bainitic Steels," *ISIJ Intl.*, Vol. 45, No. 11, 2005, pp. 1736–1740.

50. H.K.D.H. Bhadeshia and D.V. Edmonds, "Bainite in Silicon Steels: New Composition-Property Approach, Part 1," *Metal Sci.*, Vol. 17, Sept. 1983, pp. 411–419.

51. Ibid., "Bainite in Silicon Steels: New Composition-Property Approach, Part 2," *Metal Sci.*, Vol. 17, Sept. 1983, pp. 420–425.

52. V.T.T. Miihkinen and D.V. Edmonds, "Tensile Deformation of Two Experimental High-Strength Bainitic Low-Alloy Steels Containing Silicon," *Materials Sci. and Tech.*, Vol. 3, June 1987, pp. 432–440.

53. Ibid., "Fracture Toughness of Two Experimental High-Strength Bainitic Low-Alloy Steels Containing Silicon," *Materials Sci. and Tech.*, Vol. 3, June 1987, pp. 441–449.

54. J.G. Speer, D.K. Matlock, B.C. De Cooman and J.G. Schroth, "Carbon Partitioning Into Austenite After Martensite Transformation," *Acta Mat.*, Vol. 51, 2003, pp. 2611–2622.

55. A.M. Streicher, J.G. Speer, D.K. Matlock and B.C. De Cooman, "Quenching and Partitioning Response of a Si-Added TRIP Sheet Steel," *Proc. of the Int. Conf. on Advanced High-Strength Sheet Steels for Automotive Applications*, AIST, June 6–9, 2004, Winter Park, Colo., pp. 51–62.

56. G.A. Thomas, J.G. Speer and D.K. Matlock, "Considerations in the Application of the 'Quenching and Partitioning' Concept to Hot Rolled AHSS Production," *Proc. of the Intl. Conf. on New Developments in Advanced High-Strength Sheet Steels,* AIST, June 15–18, 2008, Orlando, Fla., pp. 227–236.

57. E. De Moor, J. Penning, C. Föjer, A.J. Clarke and J.G. Speer, "Alloy Design for Enhanced Austenite Stabilization via Quenching and Partitioning," *Proc. of the Intl. Conf. on New Developments in Advanced High-Strength Sheet Steels,* AIST, June 15–18, 2008, Orlando, Fla., pp. 199–207.

58. E. De Moor, J.G. Speer, D.K. Matlock, C. Föjer and J. Penning, "Effect of Si, Al and Mo Alloying on Tensile Properties Obtained by Quenching and Partitioning," *Proc. of Materials Science and Technology (MS&T) 2009*, Oct. 25–29, 2009, Pittsburgh, Pa., pp. 1554–1563.

59. E. De Moor, S. Lacroix, A.J. Clarke, J. Penning and J.G. Speer, "Effect of Retained Austenite Stabilised via Quench & Partitioning on the Strain Hardening of Martensitic Steels," *Metall. Trans. A*, Vol. 39A, 2008, pp. 2586–2595.

60. E. De Moor, J.G. Speer, D.K. Matlock, J.-H. Kwak and S.-B. Lee, unpublished research.

61. H.Y. Li, X.W. Lu, W.J. Li and X.J. Jin, "Microstructure and Mechanical Properties of an Ultrahigh-Strength 40SiMnNiCr Steel During the One-Step Quenching and Partitioning Process," *Metall. Trans. A*, Vol. 41A, 2010, pp. 1284–1300.

62. Li Wang, Weijun Feng and Wenjuan Li, "Industry Trials of C-Si-Mn Steel Treated by Q&P Concept in Baosteel," *Proc. of SAE 2010 World Congress*, SAE Intl., 2010-01-0439, Detroit, Mich., 2010.

63. G.M. Cola Jr., "Dual-Phase Flash Bainite Created in 3-Second Thermal Cycle by Water Quenching," *Proc. of the Intl. Conf. on New Developments in Advanced High-Strength Sheet Steels*, AIST, June 15–18, 2008, Orlando, Fla., pp. 105–114.

64. Ibid., "Temper-Resistant 1,600 MPa/8.7%El AISI 1020 Flash Bainite Processed Steel Made in 5 Seconds," *Proc. of Materials Science and Technology (MS&T) 2009*, Oct. 25–29, 2009, Pittsburgh, Pa., pp. 1337–1345.

65. T. Lolla, G. Cola, B. Narayanan, B. Alexandrov and S.S. Babu, "Development of Rapid Heating and Cooling (Flash Processing) Process to Produce Advanced High-Strength Steel Microstructures," *Materials Science and Technology*, 2009, in press, DOI: 10.1179/174328409X433813.

66. O. Grässel, L. Krüger, G. Frommeyer and L.W. Meyer, "High-Strength Fe-Mn-(Al,Si) TRIP/TWIP Steels Development — Properties — Application," *Int. J. Plast.*, Vol. 16, Issues 10–11, 2000, pp. 1391–1409.

67. O. Bouaziz and N. Guelton, "Modeling of TWIP Effect on Work Hardening," *Mat. Sci. Eng. A*, Vol. A319-321, 2001, pp. 246–249.

68. S. Vercammen, B. Blanpain, B.C. De Cooman and P. Wollants, "Cold Rolling Behavior of an Austenitic Fe-30Mn-3Al-3Si TWIP Steel: The Importance of Deformation Twinning," *Acta Mat.*, Vol. 52, Issue 7, 2004, pp. 2005–2012.

69. L. Bracke, G. Mertens, J. Penning, B.C. De Cooman, M. Liebherr and N. Akdut, "Influence of Phase Transformations on the Mechanical Properties of High-Strength Austenitic Fe-Mn-Cr Steel," *Metall. Trans. A*, Vol. 37A, February 2006, pp. 307–317.

70. *Proc. of the Workshop on High Mn Steels*, Nov. 3–5, 2009, Graduate Institute of Ferrous Technology, Pohang University of Science and Technology, Pohang, South Korea.

71. G. Frommeyer, U. Brüx and P. Neumann, "Supra-Ductile and High-Strength Manganese TRIP/TWIP Steels for High-Energy Absorption Purposes," *ISIJ Intl.*, Vol. 43, No. 3, 2003, pp. 438–446.

72. Y.N. Dastur and W.C. Leslie, "Mechanism of Work Hardening in Hadfield Manganese Steel," *Metall. Trans. A*, Vol. 12A, May 1981, pp. 749–759.

73. M.J. Merwin, "Microstructure and Properties of Cold Rolled and Annealed Low-Carbon Manganese TRIP Steels," *Proc. of Materials Science and Technology 2007*, Sept. 16–20, 2007, Detroit, Mich., pp. 515–536.

74. Ibid., "Low-Carbon Manganese TRIP Steels," *Proc. of THERMEC 2006*, *Materials Sci. For.*, Vols. 539–543, 2007, pp. 4327–4332.

75. Ibid., "Hot and Cold Rolled Low-Carbon Manganese TRIP Steels," *Proc. of SAE Intl. World Congress & Exhibition*, April 2007, Innovations in Steel Sheet Products and Processing, SAE Paper No. 2007-01-0336.

76. Ibid., "Microstructure and Properties of Cold Rolled and Annealed Low-Carbon Manganese TRIP Steels," *Iron & Steel Technology*, Vol. 5, No. 10, October 2008, pp. 66–84.

77. R.A. Grange and R.L. Miller, "Heat Treatment for Improving the Toughness of High-Manganese Steels," U.S. Patent 4,047,979, Sept. 13, 1977.

78. R.L. Miller, "Ultrafine-Grained Microstructures and Mechanical Properties of Alloy Steels," *Metall. Trans. A*, Vol. 3, 1972, pp. 905–912.

79. A.A. Konieczny and T. Henderson, "On Formability Limitations in Stamping and Sheared Edge Stretching," SAE Technical Paper 2007-01-0340, SAE Intl., 2007, pp. 41–50.

80. S.B. Lee, J.G. Speer, D.K. Matlock and K.G. Chin, "Analysis of Stretch-Formability Using a Ductile Fracture Model," *Proc. of the 3rd Int. Conf. on Advanced Structural Steels*, ed. H.C. Lee, The Korean Institute of Metals and Materials, Aug. 22–24, 2006, pp. 841–849.

81. A.W. Hudgins, D.K. Matlock and J.G. Speer, "Shear Failures in Bending of Advanced High-Strength Steels," *Proc. of the Intl. Deep Drawing Research Group IDDRG 2009 Intl. Conf.*, eds. B.S. Levy, D.K. Matlock and C.J. Van Tyne, June 1–3, 2009, Golden, Colo., pp. 53–64.

82. M. Walp, A. Wurm, J. Siekirk III and A. Desai, "Shear Fracture in Advanced High-Strength Steels," SAE Technical Publication, SAE Intl., 2006-01-1433.

83. H. Kim, A.R. Bandar, Y-P. Yang, J.H. Sung and R.H. Wagoner, "Failure Analysis of Advanced High-Strength Steels (AHSS) During Draw Bending," *Proc. of the Intl. Deep Drawing Research Group IDDRG 2009 Intl. Conf.*, eds. B.S. Levy, D.K. Matlock and C.J. Van Tyne, June 1–3, 2009, Golden, Colo., pp. 449–460.

84. T.B. Hilditch, S-B. Lee, J.G. Speer and D.K. Matlock, "Response to Hydrogen Charging in High-Strength Automotive Sheet Steel Products," SAE Technical Publication, SAE Intl., 2003-01-0525.

85. L. Duprez, K. Verbeken and M. Verhaege, "Effect of Hydrogen on the Mechanical Properties of Multiphase High-Strength Steels," *Proc. of the 2008 Intl. Hydrogen Conf.*, eds. B. Somerday, P. Sofronis and R. Jones, ASM Intl., pp. 62–69.

86. J.A. Ronevich, J.G. Speer and D.K. Matlock, "Hydrogen Embrittlement of Commercially Produced Advanced High-Strength Sheet Steels," *Proc. of SAE 2010 World Congress and Exhibition*, SAE Intl., April 13–15, 2010, Detroit, Mich., 2010-01-0447. ✦